Available online at www.sciencedirect.com
ScienceDirect
Journal of the European Ceramic Society 31 (2011) 1723–1731
www.elsevier.com/locate/jeurceramsoc

Spark plasma sintering of nanocrystalline $BaTiO_3$-powders: Consolidation behavior and dielectric characteristics

Songhak Yoon [a,*], Jürgen Dornseiffer [b], Yan Xiong [c], Daniel Grüner [c], Zhijian Shen [c], Shoichi Iwaya [d,e], Christian Pithan [a], Rainer Waser [a]

[a] *Institute for Solid State Research, Forschungszentrum Jülich GmbH, D-52425 Jülich, Germany*
[b] *Institute for Chemistry and Dynamics of the Geosphere, Forschungszentrum Jülich GmbH, D-52425 Jülich, Germany*
[c] *Arrhenius Laboratory, Stockholm University, SE-10691 Stockholm, Sweden*
[d] *IOM Technology Corporation, 957-0231 Shibata-shi, Japan*
[e] *Technical R&D division, NAMICS CORPORATION, 108-0074 Tokyo, Japan*

Received 29 October 2010; received in revised form 14 March 2011; accepted 20 March 2011
Available online 14 April 2011

Abstract

$BaTiO_3$ nanopowders prepared by two different wet chemical routes, one based on microemulsion-mediated synthesis (M-BT) and the other one on the alkoxide–hydroxide method (A-BT) were consolidated by spark plasma sintering (SPS). The densification process, the linear shrinkage rates and the relative densities achieved were strongly dependant on the synthetic route. The results show that fully densified $BaTiO_3$ ceramics with a grain size of about 200 nm can be obtained in both cases by controlling the sintering temperature during the SPS process. The study of dielectric properties revealed that M-BT derived ceramics show higher permittivity values compared to those obtained for A-BT. The influence of the barium/titanium ratio on the sintering behavior and the dielectric properties is discussed.
© 2011 Elsevier Ltd. All rights reserved.

Keywords: $BaTiO_3$; Spark plasma sintering; Grain growth; Dielectric properties

1. Introduction

The ferroelectric compound barium titanate ($BaTiO_3$) represents one of the most extensively studied perovskite-type oxides due to its excellent dielectric, piezoelectric and ferroelectric properties.[1] It is widely used in various electronic components including thermistors, sensors, electro-optical devices and multi-layer ceramic capacitors (MLCCs).[2,3] With the ongoing trend to miniaturization of electronic devices in general, and in MLCC industry in particular, the layer thickness of $BaTiO_3$ based dielectrics is expected to decrease continuously well below 1 μm to reach values of only a few hundreds of nm.[4]

Manufacturing MLCCs consisting of ferroelectric ultrafine or even nanocrystalline grains, however, still remain challenging, because the polarity and herewith the dielectric constant of $BaTiO_3$ generally deteriorates with decreasing grain-size, a phenomenon which is commonly referred to as "size-effect". It is often reported that downsizing the crystals dimensions of $BaTiO_3$-grains below a critical value results in the stabilization of the paraelectric and crystallographically centrosymmetric cubic, high-temperature polymorph of the perovskite lattice at the expense of the tetragonal structure, even at room temperature.[5,6] This leads in average to a reduction of the tetragonal distortion of the lattice and a decrease of the herewith connected ferroelectric polarization. Arlt et al. showed that for $BaTiO_3$ maximum values of permittivity around 5000 can be achieved at grain sizes of 0.8–1 μm.[7] Similarly, Hirata et al. reported later that the dielectric constant showed a slightly higher maximum of 5700 at a grain size of approximately 1.4 μm.[8] In any case, however, a marked decrease of the relative dielectric constant with diminishing grain-size is observed. Contrary to this, Guillemet-Fritsch et al. reported recently that ultrafine

* Corresponding author. Present address: Empa, Swiss Federal Laboratories for Materials Science and Technology Laboratory for Solid State Chemistry and Catalysis, Überlandstrasse 129, 8600 Dübendorf, Switzerland. Tel.: +41 44 823 4602; fax: +41 58 765 4019.
E-mail address: songhak.yoon@empa.ch (S. Yoon).

0955-2219/$ – see front matter © 2011 Elsevier Ltd. All rights reserved.
doi:10.1016/j.jeurceramsoc.2011.03.035

La-doped $BaTiO_3$ ceramics with an average grain size of only 250–300 nm unexpectedly show colossal permittivity values up to 10^6.[9] For a much finer grain-size of 70 nm in average Frey et al. reported that the overall dielectric constant of the ceramic was only about 2500.[10] These authors claimed the existence of a low permittivity grain-boundary region of approximately 0.8 nm thickness with a dielectric constant of 130 that surround the high permittivity ($\varepsilon_r = 4800$) ferroelectric cores of the $BaTiO_3$-grains. With decreasing grain-size the relative volume fraction occupied by the grain boundary regions increases and in consequence, because of this "dilution effect", the overall dielectric constant is lowered. Earlier studies on the size effect of ferroelectric particles like $BaTiO_3$ often suggested from the extrapolation of the reduction of the tetragonality in lattice distortion or of the Curie temperature T_c that ferroelectricity completely vanishes below a certain critical value of grain-size. In this context Frey et al. assumed according to their analysis that this critical size should be smaller than 40 nm. To answer the question of this ferroelectric limit in grain-size for nanocrystalline $BaTiO_3$ ceramics several reports have addressed the issue again experimentally. Buscaglia et al. investigated nanocrystalline $BaTiO_3$ ceramics consolidated from powders synthesized by the tubular flow method by spark plasma sintering (SPS) with a resulting average grain-size of only 50 nm. They directly evidenced weak tetragonality on the macroscopic scale by Raman-spectroscopy and showed the existence of regions that revealed local hysteric switching by piezoresponce force microscopy, while other parts in the microstructure seemed to be inactive.[11,12] Shiratori et al. described in more detail the stability of the tetragonal phase and other polymorphs of nanocrystalline $BaTiO_3$ as a function of the crystallite size and aggregation degree in loose powders, annealed and coarsened aggregates and finally sintered nanoceramics.[13–15] These results, also based on Raman-spectroscopy, clearly showed the presence of a polar structure in ceramics with an average grain-size as small as 35 nm. The comparison of the temperature dependence of their spectroscopic data for the three different microstructural conditions mentioned before, indicated, that tetragonality is stabilized in the densified polycrystalline state in contrast to crystallites of almost the same size in the free (non-aggregated but loosely agglomerated) condition. After all, the nature of the size effect and the origin and value of the critical size of $BaTiO_3$ nanocrystals is still discussed controversially since many factors, including the synthesis method of the powders and the conditions of their further thermal treatment or processing to consolidated sintered bodies affects the crystallography, mesostructure and permittivity.

To successfully densify ceramic nanopowders into consolidated solids while preserving an ultrafine microstructure, spark plasma sintering (SPS) has been proven to be one of the most effective sintering techniques. Because SPS offers the combined advantages of fast heating rates, the application of mechanical pressure, short sintering times at generally low sintering temperatures, SPS provides a valuable approach to promote densification and reduce grain coarsening during sintering of nanopowders.[16,17] Takeuchi et al. have reported that dense $BaTiO_3$ ceramics with an average grain size of less than 1 μm can be fabricated by SPS.[18] In the course of studying the sintering behavior of nanocrystalline $BaTiO_3$ powders (with an average particle size ranging between 60 and 80 nm) using SPS, Liu et al. have found the existence of a window of processing parameter within which the densification process can be kinetically separated from grain growth.[19] Deng et al. have successfully prepared dense $BaTiO_3$ ceramics with the grain size of 20 nm by SPS and the crystal structure and ferroelectric properties of nanocrystalline $BaTiO_3$ were investigated.[20,21]

Up to date, however, no publication has yet reported about SPS of $BaTiO_3$ nanopowders synthesized through microemulsion-mediated synthesis or the alkoxide–hydroxide method and the dielectric properties of the resulting ceramics.

Table 1
Crystal size, particle size, and Ba/Ti ratio for the A-BT (alkoxide–hydroxide method) and M-BT (microemulsion synthesis) powders.

Name	Crystal size[a] (nm)	Particle size[b] (nm)	Ba/Ti ratio[c]
A-BT	40	828	0.9434
M-BT	10	15	1.0021

[a] Calculated by Scherrer equation.
[b] Obtained by dynamic light scattering (DLS) measurement.
[c] Obtained by inductively coupled plasma (ICP).

2. Experimental procedures

$BaTiO_3$ nanopowders were synthesized via microemulsion-mediated synthesis or the alkoxide–hydroxide sol-precipitation method, respectively. The synthesized $BaTiO_3$ nanoparticles were aggregates of nanosized primary particles of about 40 nm in size for the alkoxide–hydroxide method and as small as 10 nm for microemulsion-mediated synthesis. Both these powders are denoted as A-BT (alkoxide–hydroxide method) and M-BT (microemulsion synthesis) respectively in the following. The experimental details of the preparation procedures and of the characteristics of the synthesized nanopowders are described in previous papers and summarized in Table 1.[22–25]

In order to densify the $BaTiO_3$ nanopowders, spark plasma sintering (SPS) has been carried out using a Dr. Sinter 2050 apparatus (SPS Syntex Inc., Sumitomo Coal Mining Co., Tokyo, Japan). SPS allows a densification at relatively low temperatures under the application of a mechanical pressure and an electrical discharge, substantially limiting coarsening of the microstructure due to the extensive grain-growth. In a typical consolidation cycle, nanopowder (1.6 g) was loaded into a graphite pressure die (inner diameter of 12 mm) which is heated up to a temperature of 600 °C via a preset heating program within 3 min. The temperature was then automatically regulated from 600 °C to the final sintering temperature (T_F) with a heating rate of 100 K/min and monitored with an pyrometer focused on the surface of the graphite die. Different sintering temperatures T_F of 950 °C, 975 °C, 1000 °C, 1025 °C and 1050 °C were applied respectively. As soon as T_F was reached an uniaxial pressure of 75 MPa was applied and the dwelling time kept was 5 min. Applying the pressure at T_F results in a finer grain structure compared to the case when the pressure is already directly applied from the beginning of the heating cycle.[26]

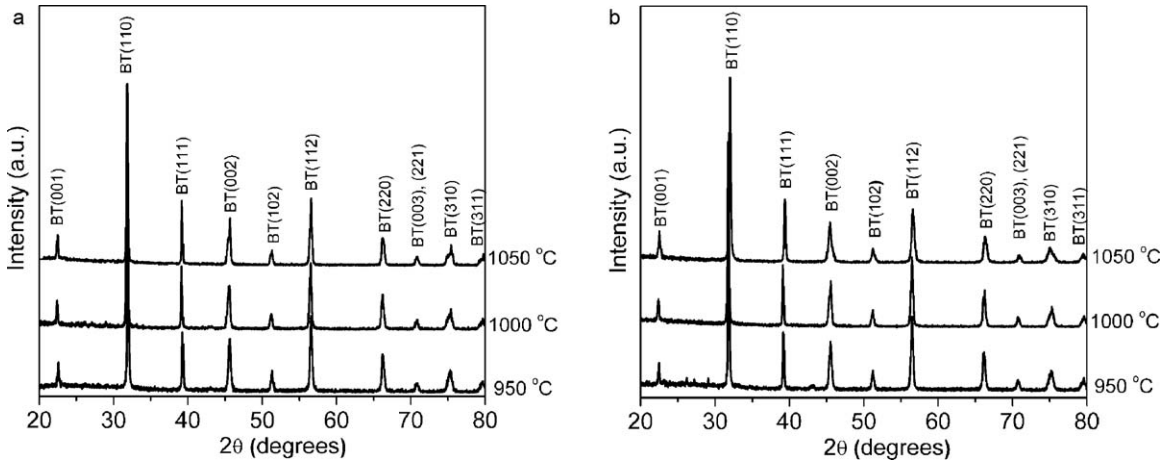

Fig. 1. X-ray diffraction patterns of compacts obtained for (a) A-BT and (b) M-BT powders after SPS (BT: $BaTiO_3$).

The sintered pellets were characterized regarding phase composition by powder X-ray diffraction (XRD, Philips X'PERT, Koninklijke Philips Electronics N.V., Amsterdam, the Netherlands) using Cu-K_α radiation with a wavelength of $\lambda = 1.5418$ Å. The respective diffraction patterns were recorded in the range from 20° to 80° (2θ) using an angular step interval of 0.02°.

The grain size and its spatial distribution in the sintered $BaTiO_3$ ceramics were investigated by field emission scanning electron microscopy (FE-SEM, LEO1530, Carl Zeiss AG, Jena, Germany) operating at an accelerating voltage of 20 kV. The average grain size (G) was then determined via the linear intercept method from micrographs of fractured surfaces of all samples, using the relationship $G = 1.5 \cdot L$, where L is the average intercept length.[27] Approximately a number of 350–500 intercepts were counted for each sample.

For the dielectric measurements, gold electrodes were deposited onto the sintered pellets by sputtering. The measurements were performed in a frequency range from 0.1 Hz to 1 MHz with an applied AC voltage of 1.5 V for temperatures between 25° and 250 °C using an impedance analyzer (Alpha Dielectric Analyzer, NOVOCONTROL Technologies GmbH & Co. KG, Hundsangen, Germany). The system used consisted of a frequency response analyzer (Solartron SI 1260, Solartron Analytical, Farnborough, U.K.) and a broadband dielectric converter (Novocontrol BDC, NOVOCONTROL Technologies GmbH & Co. KG, Hundsangen, Germany).

In order to study the stoichiometry of the as synthesized powdery products, M-BT and A-BT nanopowders were sintered at 1000 °C by SPS and additionally post-annealed at 1350 °C for 30 min in air applying a heating and cooling rate of 5 K/min respectively and investigated by XRD.

3. Results and discussions

3.1. Sintering behavior and microstructural evolution

Fig. 1 shows the X-ray diffraction patterns of some representatively selected ceramics derived from M-BT and A–BT respectively. All reflection peaks were identified to arise from $BaTiO_3$ and no other secondary phases could be found, suggesting that no detectable side reaction took place during the sintering process over the temperature range investigated (950–1050 °C).

Dilatometric linear shrinkage curves recorded for compacts of A-BT and M-BT sintered at 1000 °C are shown in Fig. 2. The shrinkage in the case of A-BT started at about 980 °C and a strong increase in the shrinkage occurred when the uniaxial pressure of 75 MPa was applied as soon as the sintering temperature of 1000 °C was reached. Then, in the course of further densification, the linear shrinkage gradually increased with the increase in dwelling time. The corresponding linear shrinkage of M-BT derived powders already starts at a temperature of about 780 °C, which is 200 K below that for A-BT, where a significant increase in densification starts. The large difference in the onset temperature of sintering is probably due to different agglomeration degrees of the raw powders (see Table 1) and the herewith related formation of initial sintering necks. The difference in sinter-activity manifests itself even more clearly in the temperature between 780 °C and 1000 °C. After pressurization the M-BT powder densifies much quicker than the A-BT–powder. In the case of M-BT densification is already almost completed within

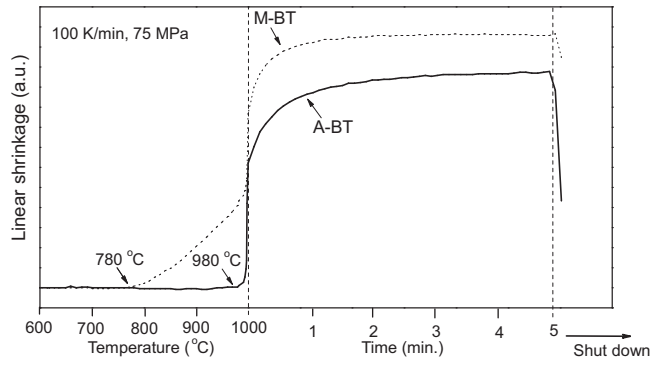

Fig. 2. Linear shrinkage rate plotted versus the temperature for compacts of A-BT and M-BT sintered at 1000 °C and a pressure of 75 MPa (heating rate between 600 °C and 1000 °C was 100 K/min). The right part of the figure shows the evolution of the shrinkage with time after applying the pressure at 1000 °C.

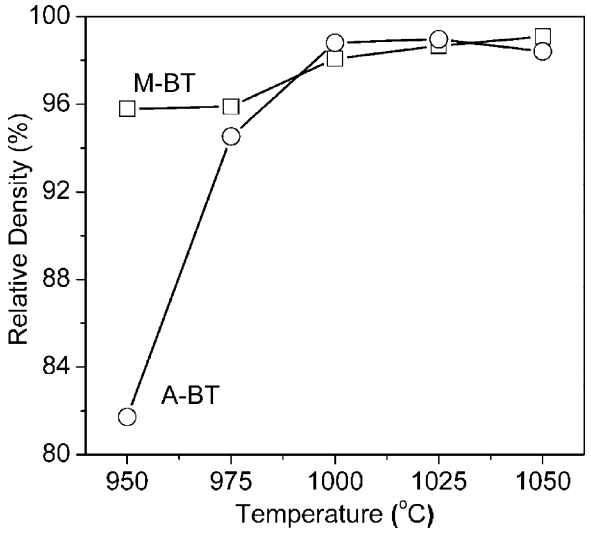

Fig. 3. Relative density of ultrafine grained $BaTiO_3$ compacts in dependence of sintering temperature.

2 min, whereas in the case of A-BT the saturation in the displacement recorded by the dilatometer can be recognized after 5 min.

Fig. 3 illustrates the densification behavior of A-BT and M-BT in more detail and shows the influence of temperature on the values of the final relative density achieved for the sintered compacts. In the case of M-BT a continuous but only relatively small increase in relative density from 95.8 to 99.1% was observed. For A-BT nanopowders, on the contrary, a sharp and rapid increase in the relative density from 81.7 to 98.8% was observed within a very narrow temperature interval of 50 K, between 950 °C and 1000 °C. A further increase in the sintering temperature above 1050 °C does not enhance the densification of the compacts. The threshold temperature above which creep or grain-boundary sliding is much higher for A-BT than for M-BT. Hague and Mayo reported that during sinter-forging of nanocrystalline zirconia, dynamic grain growth due to the applied plastic strain induced by plastic deformation can provide an additional driving force in grain growth and densification.[28] In our study, M-BT have experienced larger plastic strains in lower temperature region compared to A-BT during SPS due to the smaller initial particle size and higher surface to volume ratio.

The evolution of the microstructures with increasing sintering temperature is shown in Fig. 4. The fractured surfaces of all samples reveal nanosized grains. Channels of remaining open porosity can be recognized for A-BT compacts sintered at 950 °C (Fig. 4(a)) due to the low relative density (81.7%). However, when the sintering temperature is increased up to 1050 °C, much more densified sintered bodies can be achieved (98.8%). This enhancement in density is nevertheless accompanied by grain growth. A much higher relative density (95.8%) was obtained for M-BT compacts sintered at 950 °C. This is probably mainly due to the onset of sintering and neck formation at a temperature as low as 780 °C. However, gradual grain growth was also observed with increasing sintering temperature above 950 °C in this case. As already indicated in relation with the dilatometric linear shrinkage traces in Fig. 2, shrinkage in both, A-BT as well as M-BT compacts starts below 1000 °C: at 980 °C for A-BT and at 780 °C for M-BT. Even though primary particle sizes were very small in both cases (40 nm for A-BT and 10 nm for M-BT), it was difficult to achieve fully densified $BaTiO_3$ nanoceramics at temperatures below 1000 °C due to the tendency of the $BaTiO_3$ nanoparticles to form more or less stable agglomerates. Therefore, a further decrease of the agglomeration degree is desirable for the synthesis of nanoparticles in order to retain an even finer nano-crystalline microstructure at high density levels.

The measured grain sizes are plotted as a function of the sintering temperature in Fig. 5. Two regimes of grain growth can be distinguished. Below 1025 °C both A-BT and M-BT only show a rather small and almost linear increase of the average grain size with temperature. For A-BT this increase is relatively more pronounced, compared to M-BT. In both cases, however, below 1025 °C the average grain size remains smaller than 400 nm. On the other hand, above 1025 °C both powders have already almost

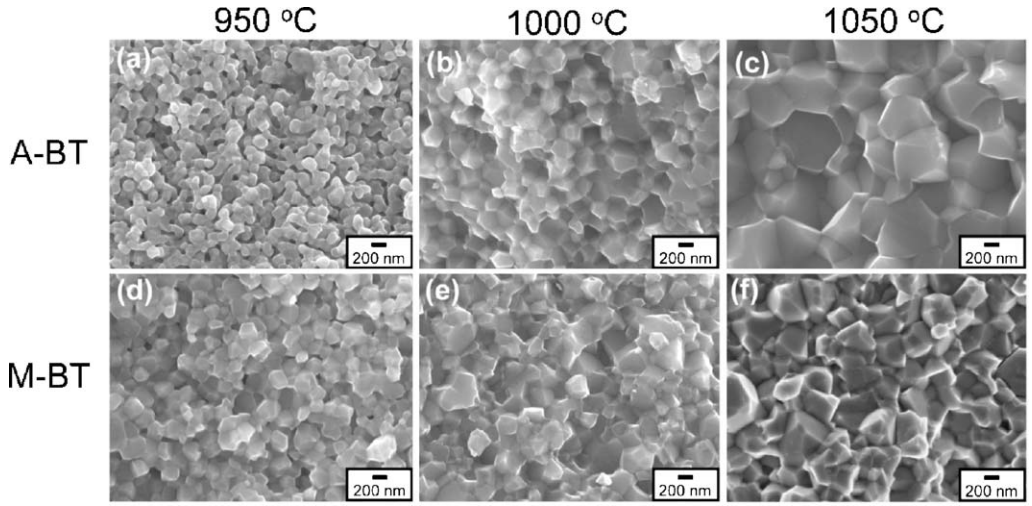

Fig. 4. SEM micrographs of A-BT ceramics (upper row (a–c)) and M-BT ceramics (lower row (d–f)) sintered at 950 °C (a and d), 1000 °C (b and e), and 1050 °C (c and f), respectively.

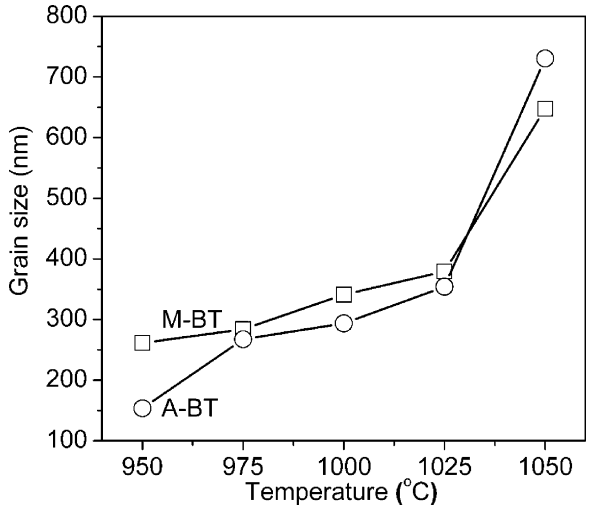

Fig. 5. Grain size of A-BT and M-BT compacts in dependence of sintering temperature.

reached the value of the theoretical density and a drastic promotion of grain growth is observed. The observed microstructures, shown in Fig. 4, reveal that homogeneous and not abnormal coarsening is taking place in this temperature regime.

Fig. 6 illustrates the two concurrent mechanisms of grain growth and densification independently from temperature in a sintering-map, in which the achieved average grain size is plotted versus the relative density. Interestingly the representation of the experimental data in this chart reveals that no significant or fundamental difference in the sintering kinetics of both powders occur during the final stages of consolidation, since the traces of the grain size dependence from density seem to follow the same tendency above the value of closed porosity (about 94%). In both cases very strong grain growth takes place just before the theoretical density is reached if the temperature is increased.

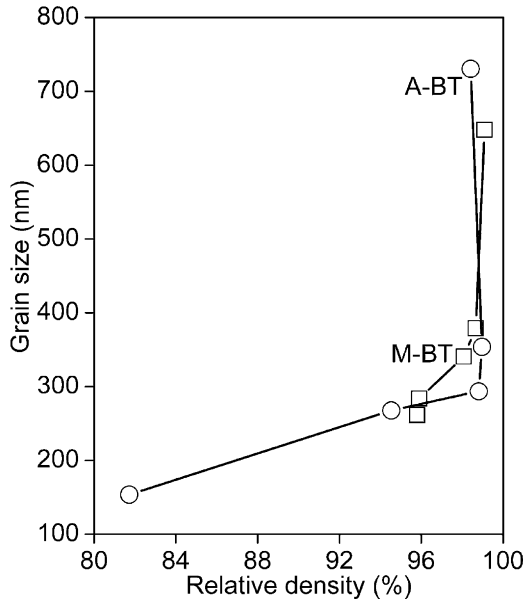

Fig. 6. Grain size as a function of density for A-BT and M-BT compacts.

3.2. Dielectric characteristics

Fig. 7 shows the frequency-dependence of permittivity for different sintering temperatures. Most of the ceramics obtained from A-BT powders had a sufficiently good stability of the permittivity within the wide frequency range from 0.1 Hz to 1 MHz, as illustrated in Fig. 7(a). The extremely low values of permittivity well below 1000 for A-BT sintered at 950 °C and 975 °C are probably due to lower densities ("dilution effect" because of low permittivity pores) as well as small grain sizes ("size effect").[29] The permittivity values increase, however, for higher sintering temperatures up to 1025 °C and thus larger densities and grain sizes. The A-BT sample sintered at 1050 °C interestingly shows a lower permittivity than that sintered at 1000 °C. An increase of the permittivity also occurs in M-BT compacts with increasing sintering temperature up to 1025 °C at low frequencies as shown in Fig. 7(b). The only exception to this trend occurs for M-BT sintered at 975 °C that shows the largest values of permittivity in all M-BT compacts. The reasons for this behavior are not understood at the moment. A very steep increase of permittivity was observed with decreasing frequency for M-BT derived ceramics sintered below 1000 °C having a grain size of 350 nm or less. This increase is particularly steep for M-BT powders sintered at 950 °C. Possibly this polarization contribution arises not only from the intrinsic dielectric response of the crystal lattice but also from extrinsically induced mechanisms, such as space charge layers.

The dielectric losses (loss tangent, $\tan\delta$) for A-BT and M-BT as a function of frequency at room temperature are shown in Fig. 8. The A-BT samples sintered at 950 °C and 975 °C revealed a strong dependence of the dielectric losses from frequency. With increasing sintering temperatures, however, reduced frequency dependence is observed (Fig. 8(a)), which is associated with a lower porosity and enhanced densification and grain growth.[8] The M-BT samples also show the development of almost frequency independent losses for high values of the sintering temperatures. Most of the M-BT samples show higher values of dielectric losses compared to those obtained for A-BT, as shown in Fig. 8(b). For the fully densified samples the dielectric losses lie between 10^{-2} and 10^{-1} for A-BT and M-BT.

Typical permittivity–temperature characteristics reflecting ferroelectric behavior were obtained for both A-BT and M-BT samples and Fig. 9 shows representative examples of the temperature dependence of permittivity at 1 kHz for A-BT sintered at 1025 °C (99% density and 354 nm grain-size) and M-BT sintered at 975 °C (96% density and 284 nm grain-size), both cases having a comparable microstructure. The maximum dielectric constant appears, as expected at around 115 °C, which corresponds to the Curie-temperature of $BaTiO_3$, where the transition between the ferroelectric (crystallographic tetragonal polymorph) and the high-temperature paraelectric (crystallographic cubic polymorph) occurs.[30] Above the Curie point, a proportional relation between the reciprocal permittivity and temperature holds for both A-BT and M-BT samples (inset in Fig. 9), corresponding to the Curie–Weiss law, $\varepsilon = C/(T - T_0)$, where ε is the permittivity of material, C the Curie constant, T the temperature and T_0 the Curie–Weiss temperature.

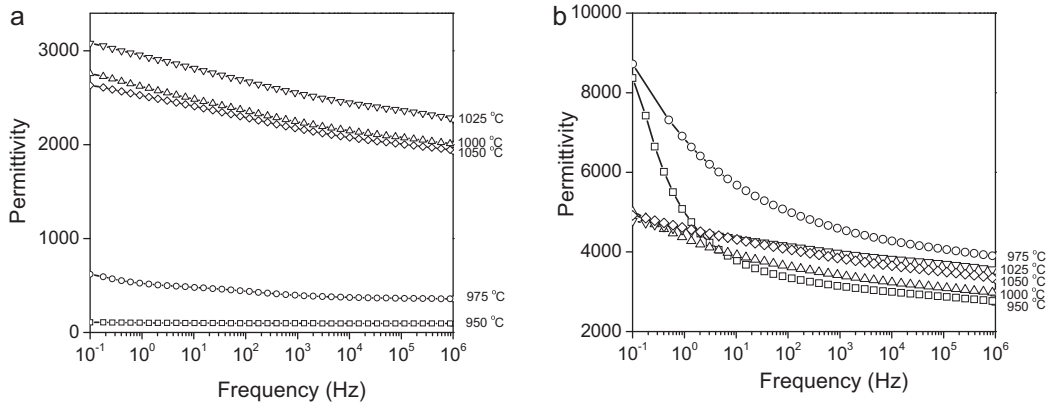

Fig. 7. Frequency dependence of permittivity for (a) A-BT and (b) M-BT compacts measured at room temperature.

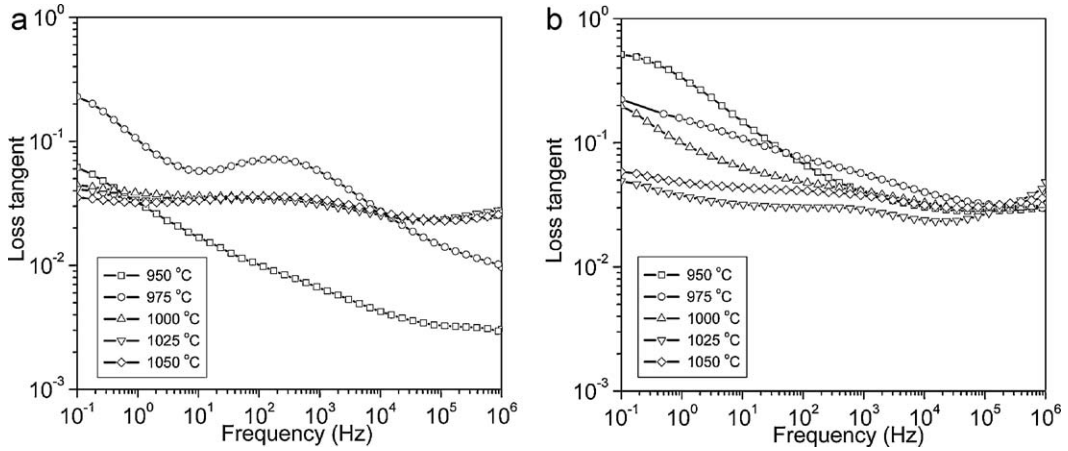

Fig. 8. Frequency dependence of loss tangent for (a) A-BT and (b) M-BT compacts measured at room temperature.

($C = 1.55 \cdot 10^5$ K and $T_0 = 350$ K for A-BT and $C = 2.61 \cdot 10^5$ K and $T_0 = 349$ K for M-BT, respectively). It should be noted that interestingly the overall permittivity is almost twice as high for M-BT compared to A-BT, although the microstructures are comparable with respect to density and grain-size, M-BT showing, however, a slightly smaller density and average grain-size than A-BT.

Fig. 10 represents the grain size dependence of permittivity for A-BT and M-BT in comparison to further data on the size-effect in sintered $BaTiO_3$ that has been published by other authors previously and that can be found in the literature.[7,10,31–35] For A-BT, a sudden drop of permittivity with decreasing grain size occurs from 294 nm (sintering at 1000 °C)

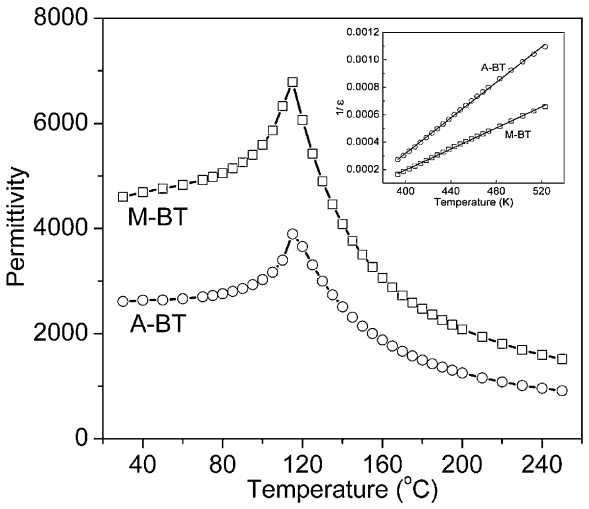

Fig. 9. Temperature dependence of permittivity for A-BT sintered at 1025 °C (99% density, 354 nm grain-size) and M-BT sintered at 975 °C (96% density, 284 nm grain-size) measured at 1 kHz.

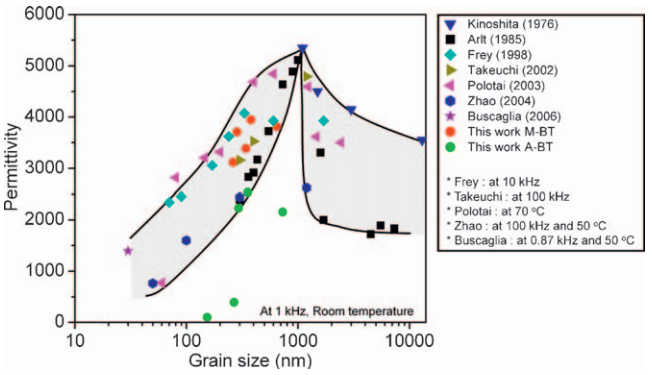

Fig. 10. Grain size dependence of permittivity for A-BT and M-BT in comparison to further data in the literatures.

down to 268 nm (sintering at 975 °C). For all M-BT sintered bodies, however, the dielectric permittivity was much higher than those obtained for A-BT. It is important to note here again that even at comparable values of the grain size (268 nm for A-BT and 261 nm for M-BT, respectively) and density (94.5% of the theoretical density for A-BT and 95.9% for M-BT) at the same time very large differences in permittivity depending on the synthetic route of nanoparticles are observed.

4. Discussion

The sintering behavior of nanocrystalline $BaTiO_3$ powders synthesized by the alkoxide–hydroxide method (A-BT) and by microemulsion-mediated synthesis (M-BT) is quite different. This discrepancy in sintering behavior can be originated from the difference in particle size. It must be stressed, however, that the degree of agglomeration usually also strongly affects sintering as a further factor besides the initial particle size. Agglomerates in ceramic powders often cause an inhomogeneous pore distribution in green compacts, resulting in persisting porosity even in the sintered body. This hampers full consolidation and, henceforth, sintering has to occur at a higher temperature in order to achieve high densification.[36] The clear advantages of nanopowders, such as the higher sinter activity or the possibility of realizing ultrafine microstructures are often put into question because of the strong tendency to form hard agglomerates as the particle sizes decreases below 100 nm. For this reason there is a vigorous demand for the development of only loosely agglomerated powders and of means allowing to control the spontaneous agglomeration of nanoparticles during wet chemical processing such as the synthesis through the hydrothermal, the sol–gel, the microemulsion, and the alkoxide–hydroxide approach.

As already mentioned Liu et al. found the existence of a kinetic window within which the densification process of nanocrystalline $BaTiO_3$ powders (average initial particle size 60–80 nm) could be separated from grain growth.[19] In the present study, the initial particle size of the $BaTiO_3$ nanopowders was about 10 and 40 nm, respectively, and such a kinetic window was not observed. It should be noted in this context, that all grain sizes measured for our sintered A-BT and M-BT were significantly smaller than the ones reported previously for the case where abnormal grain growth occurred and therefore it can be concluded that the present data lie within or below the kinetic window reported by Liu et al. Presumably, both A-BT and M-BT experience grain growth without densification during SPS if a higher sintering temperature is applied.

The critical grain size where permittivities begin to decrease drastically upon microstructural refinement was found to be around 300 nm for A-BT. For M-BT permittivity remained almost constant down to this value and no critical value could be found experimentally. This difference in permittivity is believed to result from factors affected by the synthetic approach, such as for instance the concentration of point defects. It is well known that the sintering behavior of $BaTiO_3$ is greatly influenced by stoichiometry and the occupancy balance of the cationic sites in the perovskite lattice.[37] Pinceloup et al. proved the existence of a narrow stoichiometry range of the Ba/Ti ratio from 0.995 to 1.000 in which optimum sintering behavior and electrical properties of hydrothermally synthesized $BaTiO_3$ nanopowders can be obtained.[38]

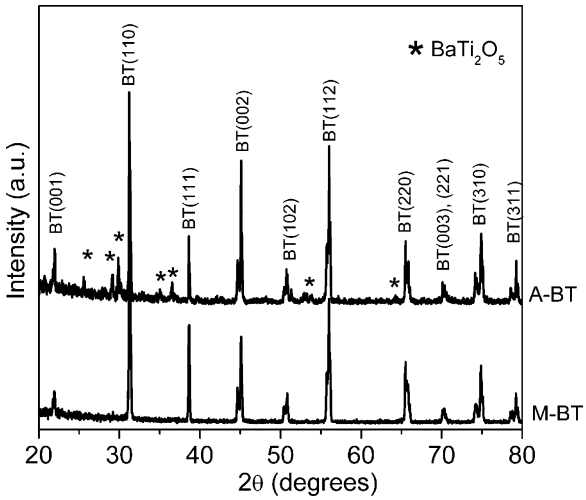

Fig. 11. X-ray diffraction patterns of SPSed A-BT and M-BT compacts annealed at 1350 °C for 30 min. These compacts were sintered at 1000 °C by SPS before annealing (BT: $BaTiO_3$).

In order to verify the stoichiometry of the synthesized $BaTiO_3$ nanopowders of the present study, XRD on post-sintering annealed ceramics was conducted. Fig. 11 shows XRD patterns of A-BT and M-BT compacts (consolidated by SPS at 1000 °C) that were annealed at 1350 °C for 30 min. For M-BT, all reflection peaks could be indexed on the basis of the tetragonal $BaTiO_3$ crystal structure. According to XRD no secondary phases form during annealing, indicating that these M-BT ceramics exist in the pure stoichiometric composition. However, in the case of A-BT Bragg-reflections of $BaTi_2O_5$ (JCPDS 34-0133) as a secondary phase were identified beside $BaTiO_3$ upon annealing, which proves the presence of fluctuations in stoichiometry. Fig. 1 shows that the content of secondary phases after sintering, if present at all, is well below the XRD detection limit (<1 vol%) for both SPSed A-BT and M-BT compacts. In the case of the alkoxide method, however, hydroxyl ions are usually incorporated into the lattice, resulting in cationic vacancies on tempering.[39,40] It is expected that due to the presence of barium vacancies in A-BT, Ti-rich secondary phases can be formed during annealing. The change of the local stoichiometry can be one main factor which affects sintering and the dielectric behavior of the nanocrystalline $BaTiO_3$ ceramics from A-BT.

The different dielectric properties of the A-BT and M-BT can be also probably originated from the existence of a non ferroelectric grain boundary layer, so-called “dead layer” which determines a progressive suppression of permittivity in $BaTiO_3$ ceramics.[10,34,35] The thickness of this layer is related to the Ba/Ti ratio and in the A-BT ceramics there is probably thicker dead layer due to the significant Ti excess as evidenced in Table 1 compared to M-BT. In this case an amorphous Ti-rich layer might be also present at grain boundaries which would give a strong impact on grain growth and densification, as defect nature and defect concentration in $BaTiO_3$ are strongly dependent on Ba/Ti ratio. Thus, further investigations on the effect of dead layer will

be carried out, which might provide fundamental understanding of the origin of the different dielectric properties on the A-BT and M-BT ceramics.

5. Summary

Nanocrystalline $BaTiO_3$ powders prepared with microemulsion-mediated synthesis (M-BT) and alkoxide–hydroxide method (A-BT) have been successfully densified by SPS. In-situ measurement of the linear shrinkage behavior shows that in the case of M-BT sintering is initiated at much lower temperatures compared to A-BT due to the small initial particles size. During SPS, both the processes of grain growth and densification proceeded simultaneously below 1000 °C whereas above approximately 1000 °C the sintering behavior is mainly governed by grain growth rather than densification for both A-BT and M-BT powders. The study of the dielectric properties revealed typical permittivity–temperature characteristics. M-BT, however, shows significantly higher values of permittivity compared to A-BT. Possibly the rather poor control of stoichiometry during synthesis in the case of A-BT affects the dielectric behavior of the resulting ceramics.

Acknowledgements

This work was supported by the Korea Research Foundation Grant funded by the Korean Government (KRF-2007-D00124). S. Yoon acknowledges support from COST Action 539 (COST-STSM-539-03589) of the European Union. NAMICS Corporation, Niigata (Japan) is gratefully acknowledged for financial support within a common collaboration project. The authors are grateful to Dr. Wessel Egbert for FE-SEM and to Dr. Detlev Hennings for helpful discussion and comments.

References

1. Pithan C, Hennings D, Waser R. Progress in the synthesis of nanocrystalline $BaTiO_3$ powders for MLCC. *Int J Appl Ceram Technol* 2005;**1**:1–14.
2. Moulson AJ, Herbert JM. Temperature-sensitive resistors in electroceramics. In: *Materials, properties, applications*. 2nd ed. West Sussex, UK: John Wiley & Sons Ltd.; 2003. p. 159–73.
3. Phule PP, Risbud SH. Low-temperature synthesis and processing of electric materials in the $BaO–TiO_2$ system. *J Mater Sci* 1990;**25**:1169–83.
4. Randall M, Skamser D, Kinard T, Qazi J, Tajuddin A, Trolier-McKinstry S, et al. Thin film MLCC. In: *CARTS USA 2007 symposium proceedings, Albuquerque, NM*. 2007. p. 403–15.
5. Uchino K, Sadanaga E, Hirose T. Dependence of the crystal structure on particle size in barium titanate. *J Am Ceram Soc* 1989;**72**:1555–8.
6. Tsunekawa S, Ishikawa K, Li ZQ, Kawazoe Y, Kasuya A. Origin of anomalous lattice expansion in oxide nanoparticles. *Phys Rev Lett* 2000;**85**:3440–3.
7. Arlt G, Hennings D, With G. Dielectric properties of fine-grained barium titanate ceramics. *J Appl Phys* 1985;**58**:1619–25.
8. Hirata Y, Nitta A, Sameshima S, Kamino Y. Dielectric properties of barium titanate prepared by hot isostatic pressing. *Mater Lett* 1996;**29**:229–34.
9. Valdez-Nava Z, Guillemet-Fritsch S, Tenailleau Ch, Lebey T, Durand B, Chane-Ching JY. Collosal dielectric permittivity of $BaTiO_3$-based nanocrystalline ceramics sintered by spark plasma sintering. *J Electroceram* 2009;**22**:238–44.
10. Frey MH, Xu Z, Han P, Payne DA. The role of interfaces on an apparent grain size effect on the dielectric properties for ferroelectric barium titanate ceramics. *Ferroelectrics* 1998;**206**:337–53.
11. Buscaglia MT, Buscaglia V, Viviani M, Petzelt J, Savinov M, Mitoseriu L, et al. Ferroelectric properties of dense nanocrystalline $BaTiO_3$ ceramics. *Nanotechnology* 2004;**15**:1113–7.
12. Buscaglia V, Buscaglia MT, Viviani M, Mitoseriu L, Nanni P, Trefiletti V, et al. Grain size and grain boundary-related effects on the properties of nanocrystalline barium titanate ceramics. *J Eur Ceram Soc* 2006;**26**:2889–98.
13. Shiratori Y, Pithan C, Dornseiffer J, Waser R. Raman scattering studies on nanocrystalline $BaTiO_3$. Part I. Isolated particles and aggregates. *J Raman Spectrosc* 2007;**38**:1288–99.
14. Shiratori Y, Pithan C, Dornseiffer J, Waser R. Raman scattering studies on nanocrystalline $BaTiO_3$. Part II. Consolidated polycrystalline ceramics. *J Raman Spectrosc* 2007;**38**:1300–6.
15. Kiefer W. Recent advances in linear and nonlinear raman spectroscopy II. *J Raman Spectrosc* 2008;**39**:1710–25.
16. Viswanathan V, Laha T, Balani K, Agarwal A, Seal S. Challenges and advances in nanocomposite processing techniques. *Mater Sci Eng R* 2006;**54**:121–286.
17. Shen Z, Peng H, Liu J, Nygren M. Conversion from nano- to micron-sized structures: experimental observations. *J Eur Ceram Soc* 2004;**24**:3447–52.
18. Takeuchi T, Tabuchi M, Kageyama H. Preparation of dense $BaTiO_3$ ceramics with submicrometer grains by spark plasma sintering. *J Am Ceram Soc* 1999;**82**:939–43.
19. Liu J, Shen Z, Nygren M, Su B, Button TW. Spark plasma sintering behavior of nano-sized (Ba, Sr) TiO_3 powders: determination of sintering parameters yielding nanostructured ceramics. *J Am Ceram Soc* 2006;**89**:2689–94.
20. Deng X, Wang X, Wen H, Kang A, Gui Z, Li L. Phase transitions in nanocrystalline barium titanate ceramics prepared by spark plasma sintering. *J Am Ceram Soc* 2006;**89**:1059–64.
21. Deng X, Wang X, Wen H, Chen L, Chen L, Li L. Ferroelectric properties of nanocrystalline barium titanate ceramics. *Appl Phys Lett* 2006;**88**:252905.
22. Yoon S, Baik S, Kim MG, Shin N, Kim I. Synthesis of tetragonal barium titanate nanoparticles via alkoxide–hydroxide sol-precipitation: effect of water addition. *J Am Ceram Soc* 2007;**90**:311–4.
23. Pithan C, Shiratori Y, Waser R, Dornseiffer J, Haegel FH. Preparation, processing and characterization of nano-crystalline $BaTiO_3$ powders and ceramics derived from microemulsion-mediated synthesis. *J Am Ceram Soc* 2006;**89**:2908–16.
24. Yoon S, Kim K, Baik S. Route for the synthesis of size tunable agglomeration-free barium strontium titanate nanoparticles synthesis using ultrasonic spray nozzle system. *J Am Ceram Soc* 2010;**93**:998–1002.
25. Yoon S, Dornseiffer J, Schneller T, Hennings D, Iwaya S, Pithan C, et al. Percolative $BaTiO_3$–Ni composite nanopowders from alkoxide-mediated synthesis. *J Eur Ceram Soc* 2010;**30**:561–7.
26. Shen Z, Johnsson M, Zhao Z, Nygren M. Spark plasma sintering of alumina. *J Am Ceram Soc* 2002;**85**:1921–7.
27. Wurst JC, Nelson JA. Lineal intercept technique for measuring grain size in two-phase polycrystalline ceramics. *J Am Ceram Soc* 1972;**55**:109.
28. Hague DC, Mayo MJ. Sinter-forging of nanocrystalline zirconia 1. Experimental. *J Am Ceram Soc* 1997;**80**:149–56.
29. Kuwabara M, Takahashi S, Shimooka H. Preparation of monolithic barium titanate xerogls by sol–gel processing and the dielectric properties of their sintered bodies. *Appl Phys Lett* 1995;**66**:1704–6.
30. Harwood MG, Popper P, Rushman DF. Curie point of barium titanate. *Nature* 1947;**160**:58–9.
31. Kinoshita K, Yamaji A. Grain-size effects on dielectric properties in barium titanate ceramics. *J Appl Phys* 1976;**47**:371–3.
32. Takeuchi T, Capiglia C, Balakrishnan N, Takeda Y, Kageyama H. Preparation of fine-grained $BaTiO_3$ ceramics by spark plasma sintering. *J Mater Res* 2002;**17**:575–81.
33. Polotai A, Ragulya AV, Randall CA. Preparation and size effect in pure nanocrystalline barium titanate ceramics. *Ferroelectrics* 2003;**288**:93–102.
34. Zhao Z, Buscaglia V, Viviani M, Buscaglia MT, Mitoseriu L, Testino A, et al. Grain-size effects on the ferroelectric behavior of dense nanocrystalline $BaTiO_3$ ceramics. *Phys Rev B* 2004;**70**:024107.

35. Buscaglia MT, Viviani M, Buscaglia V, Miltoseriu L, Testino A, Nanni P, et al. High dielectric constant and frozen marcoscopic polarization in dense nanocrystalline $BaTiO_3$ ceramics. *Phys Rev B* 2006;**73**:064114.
36. Lange FF. Sinterability of agglomerated powders. *J Am Ceram Soc* 1984;**67**:83–9.
37. Anderson HU. Influence of Ba/Ti ratio on the initial sintering kinetics of $BaTiO_3$. *J Am Ceram Soc* 1973;**56**:605–6.
38. Pinceloup P, Courtois C, Leriche A, Thierry B. Hydrothermal synthesis of nanometer-sized barium titanate powders: control of barium/titanium ratio, sintering and dielectric properties. *J Am Ceram Soc* 1999;**82**: 3049–56.
39. Hennings D, Schreinemacher S. Characterization of hydrothermal barium titanate. *J Eur Ceram Soc* 1992;**9**: 41–6.
40. Viviani M, Buscaglia MT, Testino A, Buscaglia V, Bowen P, Nanni P. The influence of concentration on the formation of $BaTiO_3$ by direct reaction of $TiCl_4$ with $Ba(OH)_2$ in aqueous solution. *J Eur Ceram Soc* 2003;**23**:1383–90.